Article

The critical role of membralin in postnatal motor neuron survival and disease

Bo Yang[1], Mingliang Qu[1], Rengang Wang[1], Jon E Chatterton[1], Xiao-Bo Liu[2], Bing Zhu[1], Sonoko Narisawa[1], Jose Luis Millan[1], Nobuki Nakanishi[1], Kathryn Swoboda[3], Stuart A Lipton[1, 4] & Dongxian Zhang[1]

These authors contributed equally to this work.
Bo Yang and Mingliang Qu

[1]Neuroscience and Aging Research Center, Sanford-Burnham Medical Research Institute, La Jolla, California, USA.
[2]Electron Microscopy Laboratory, Department of Pathology and Laboratory Medicine, School of Medicine, University of California, Davis, California, USA.
[3]Department of Neurology, Massachusetts General Hospital, Boston, Massachusetts, USA.
[4]Department of Neurosciences, University of California, San Diego, School of Medicine, La Jolla, California, USA.

Present address:
Eugenom, Inc., San Diego, California, USA
Bo Yang

Shanghai Yuanqi Clinical Lab Ltd.

Mingliang Qu

Correspondence should be addressed to Dongxian Zhang (dzhang@sbmri.org)

Abstract

Hitherto, membralin has been a protein of unknown function. Here, we show that membralin mutant mice manifest a severe and early-onset motor neuron disease in an autosomal recessive manner, dying by postnatal day 5-6. Selective death of lower motor neurons, including those innervating the limbs, intercostal muscles, and diaphragm, are predominantly responsible for this fatal phenotype. Neural expression of a membralin transgene completely rescues membralin mutant mice. Mechanistically, we show that membralin interacts with Erlin2, an endoplasmic reticulum (ER) membrane protein that is located in lipid rafts and known to be important in ER-associated protein degradation (ERAD). Accordingly, the degradation rate of ERAD substrates is attenuated in cells lacking membralin. Membralin mutations or deficiency in mouse models induce ER stress, rendering neurons more vulnerable to cell death. Our study reveals a critical role of membralin in motor neuron survival and suggests a novel mechanism for early-onset motor neuron disease.

Introduction

The ER is a membrane-enclosed cellular organelle that plays an essential role in the folding of membrane-bound and secreted proteins, synthesis of lipids and sterols, and storage of free Ca^{2+}. ER stress is often triggered by the accumulation of unfolded proteins due to pathological conditions such as DNA sequence mutations, transcriptional and translational errors, or protein folding failure (Kim et al., 2008; Lin et al., 2008). Mammalian cells have evolved an intricate system with multiple signaling pathways to respond to ER stress, collectively termed the unfolded protein response (UPR) (Kim et al., 2008; Lin et al., 2008; Walter and Ron, 2011). If unchecked, ER stress eventually causes cell death, including neuronal death in neurodegenerative diseases (Hetz and Mollereau, 2014; Lindholm et al., 2006; Scheper and Hoozemans, 2009).

Increased ER stress is thought to play an early role in motor neuron diseases, including amyotrophic lateral sclerosis (ALS) and Charcot-Marie-Tooth (CMT) (Atkin et al., 2006; Kanekura et al., 2009; Nagata et al., 2007; Nishitoh et al., 2008; Saxena et al., 2009). Manifestations and consequences of ER stress have been studied in the pathogenesis of SOD1 mutant mice, a commonly used model of ALS that expresses mutant human SOD1 protein as found in some inherited forms of ALS (Atkin et al., 2006; Kanekura et al., 2009; Saxena et al., 2009). Many ER stress-related molecules are up-regulated in SOD1 mice at an early stage of the disease, and some are specific to motor neurons (Atkin et al., 2006; Ito et al., 2009; Kikuchi et al., 2006; Nagata et al., 2007; Saxena et al., 2009; Tobisawa et al., 2003). In addition, reduction in the ER co-chaperone SIL1 has been found to be associated specifically with ER stress-prone, fast-

fatigable motor neurons (Filezac de L'Etang et al., 2015). ER up-regulation of the UPR and aberrant modification of protein disulfide isomerase also occur in human tissues from sporadic ALS (Atkin et al., 2008; Walker et al., 2010). Our studies on the activation of the type I interferon signaling in astrocytes at pre-symptomatic stages of SOD1 mice also suggest that ER stress in motor neurons may play a crucial role in disease onset (Wang et al., 2011). Moreover, genetic interruption of UPR signaling molecules, such as XBP-1 or ASK1, protects motor neurons in SOD1 mutant mice (Hetz and Mollereau, 2014; Nishitoh et al., 2008). It has been suggested that the unusually heavy metabolic demand of motor neurons may make them particularly susceptible to ER stress (Carrascal et al., 2005; Li et al., 2005; Vinay et al., 2000). Importantly, ER stress inhibitors such as salubrinal, guanabenz, and sphin1, delay disease onset and prolong the survival of these mutant mice (Das et al., 2015; Jiang et al., 2014; Saxena et al., 2009; Wang et al., 2014). This finding suggests that ER stress-related molecules may represent rational drug targets for motor neuron diseases.

Previously, membralin had been predicted by genome sequencing to encompass an open reading frame (*orf61* in mouse and *c19orf6* in human), but the function of the encoded protein has heretofore remained unknown. *Orf61* is highly conserved and found in the genome of most species except yeast and bacteria. cDNAs for membralin have been cloned from human and mouse tissues (Andersson and von Euler, 2002; Chen et al., 2005), and the protein encoded by *orf61* was named membralin because it was predicted to be a membrane protein (Andersson and von Euler, 2002). Given the absence of known protein domains, membralin may represent a novel class of proteins.

Here, we discovered during our cloning and characterization of the glutamate receptor subunit 3B gene (GluN3B, formerly designated NR3B (Chatterton et al., 2002; Matsuda et al., 2002; Nishi et al., 2001)) that the 3' end of the GluN3B gene overlaps with the 3' end of the membralin gene on the opposite strand. Thus, our GluN3B knockout mice also carry a C-terminal truncation of membralin. We observed that GluN3B/membralin C-terminal double-knockout (DKO) mice die at postnatal day 5-6 of paresis due to severe motor neuron degeneration. Transgenic expression of membralin, but not GluN3B, rescued the phenotypes of DKO mice. Additionally, we generated membralin-specific knockout mice and found that they phenocopied the DKO mice. These data suggest that membralin plays a critical role in motor neuron survival. We also demonstrate that membralin interacts with Erlin2, a protein that is enriched in ER lipid rafts and important for ER-associated protein degradation (ERAD) (Browman et al., 2006; Ikegawa et al., 1999). Additionally, neurons from membralin mutant mice display increased basal ER stress and increased vulnerability to ER stress-inducing agents. Our discovery that membralin mutations result in motor neuron disease provides mechanistic insight into pathophysiology and may offer a novel target for therapy.

Results

Membralin knockout mice manifest severe motor neuron loss

We generated GluN3B-deficienct mice by deletion of the 8-kb region encoding the entire GluN3B gene and found that it also resulted in partial deletion of membralin **(Figure 1-figure supplement 1)**. Sequence analysis confirmed that the translation frame of the

altered membralin transcript in null mice terminates 147 nucleotides (nts) beyond the end of partial exon XI, resulting in a slightly truncated membralin protein with 49 unrelated amino-acid (aa) residues replacing the WT 89 C-terminal aa residues. Thus, our targeting strategy generated a GluN3B/membralin C-terminal DKO mouse line.

DKO mice appeared normal at birth, but unexpectedly died at postnatal day 5-6 (P5-6). The motor function of these mice was indistinguishable from WT or heterozygous littermates during the first three postnatal days, but motor strength was severely impaired thereafter, preceding death. DKO mice were also significantly smaller than WT and heterozygous littermates (**Figure 1A**), but displayed normal gross anatomy and histology in the brain (**Figure 1- figure supplement 2**), visceral organs, and skeletal muscle.

As DKO mice showed signs of paresis, we conducted histological examination of motor neurons in the lumbar spinal cord using the motor neuron-specific marker, Hb9. The numbers of motor neurons in DKO mice was unchanged at P0 and P3, but reduced by 40% at P5, compared to littermate WT controls (**Figure 1B,C**). The remaining motor neurons appeared smaller than those of WT mice. Motor neuron loss and surrounding astrogliosis were also apparent in the cervical spinal cords of P5 DKO mice (**Figure 1D**). We next examined Isg15 expression (interferon-induced 17 kDa protein), which is thought to play a role in innate immunity and is up-regulated at both pre- and post-symptomatic stages in a mouse model of amyotrophic lateral sclerosis (ALS) (Wang et al., 2011). WT mice manifested minimal Isg15 expression throughout the brain and spinal cord. In contrast, by P3, DKO mice had increased Isg15 expression in the ventral horn of the cervical and lumbar enlargement of the spinal cord (**Figure 1- figure**

supplement 3A). By P5, DKO mice showed increased Isg15 expression in additional areas containing primary motor neurons, with highest expression in the ventral horn of all segments of the spinal cord and moderate expression in the facial nucleus of the brainstem (**Figure 1- figure supplement 3A,B**). No Isg15 expression was detectable in other brain areas, even in late-stage DKO mice. These results suggest that motor neurons are progressively injured in DKO mice, starting with those in the spinal cord. Since the normal process of programmed cell death in embryonic motor neurons is complete at birth (Lance-Jones, 1982), the loss of motor neurons in DKO mice was most likely due to cellular events occurring perinatally.

To confirm specific loss of motor neurons in DKO mice, we examined the spinal roots of the lumbar spinal cord by electron microscopy. Motor neuron axons in the ventral root of DKO mice showed advanced degeneration (**Figure 1E**), whereas sensory neuron axons in the dorsal root were intact (**Figure 1F**). Under high magnification of motor neurons, we saw intra-axonal vacuoles and the loss of axoplasm (**Figure 1G**), as well as disintegrated myelin and amorphous lipids (**Figure 1H**), as typically seen in Wallerian degeneration. The percentage of degenerated axons in the ventral root of DKO mice reached 48.0 ± 4.1% by P5, which was significantly greater ($P < 0.01$) than in WT mice (8.6 ± 1.5%) (**Figure 1I**). In contrast, the percentage of degenerated axons in the dorsal root of DKO mice (10.5 ± 1.9%) was similar to that of the WT ventral root, consistent with the normal background level of axonal degeneration that occurs during development. Moreover, the sensory afferent terminals in the spinal cord of DKO mice appeared normal (**Figure 1- figure supplement 4A**). In contrast, we found degeneration of phrenic motor nerve fibers and terminals in P5 DKO mice (**Figure**

1- figure supplement 4B). These results further confirm the selective death of motor neurons in DKO mice, potentially leading to respiratory failure due to loss of motor neuron innervation of the intercostal muscles and diaphragm. Taken together, our DKO mice present a phenotype of early-onset and apparently selective motor neuron degeneration.

Causality of membralin deletion in motor neuron degeneration

Since both membralin and GluN3B are mutated in DKO mice, we needed to determine which gene was responsible for the motor neuron degeneration. Therefore, we tested whether transgenically-expressed intact membralin or GluN3B could rescue DKO mice. We generated a transgenic mouse line carrying full-length membralin under the control of the murine *prion* promoter, followed by internal ribosome entry site (IRES) and enhanced green fluorescent protein (EGFP) cDNA sequences (**Figure 2A**). The membralin transgenic mice [Tg(membralin)] were fertile, normal in size, and did not display any gross physical or behavioral abnormalities compared with their littermate controls. When Tg(membralin) mice were crossbred with DKO mice, the DKO/Tg(membralin) mice were apparently normal, manifesting neither paresis nor premature death (**Figure 2B**). Thus, the membralin transgene rescued DKO mice, even though membralin mRNA levels remained somewhat lower than in WT mice (**Figure 2C**). GFP immunostaining in the ventral horn of the spinal cord showed that membralin/GFP transgene expression was predominantly neuronal, although we could not rule out relatively weak expression in glial cells (**Figure 2- figure supplement 1**). The DKO/Tg (membralin) mice showed no sign of motor defects or motor neuron loss, despite the absence of GluN3B expression (**Figure 2D**). In contrast, the GluN3B

186 transgene did not rescue DKO mice (**Figure 2- figure supplement 2**), and GluN3B KO
187 mice generated by deleting the first exon did not show any defect in motor neurons
188 (Niemann et al., 2007). Taken together, these findings are consistent with the
189 hypothesis that loss of intact membralin in DKO mice causes motor neuron
190 degeneration.

191 Since heterozygous DKO mice did not manifest motor defects, expression of the
192 truncated form of membralin appears to lack any deleterious effect. This conclusion is
193 also supported by results from a second membralin knockout (KO) mouse line we
194 generated using a gene trapping strategy (**Figure 3A**). RT-PCR experiments using
195 primers from exon 1 and 2 further confirmed that homozygous mice carrying
196 membralin/trapping vector alleles did not express membralin mRNAs with sequences
197 beyond exon 2. Membralin protein was also reduced in heterozygotes and absent in
198 homozygotes. These membralin KO mice phenocopied the DKO mice in motor defects,
199 with ~50% motor neuron loss preceding death around P5 (**Figure 3B,C**).

200 **Membralin resides in the ER membrane and interacts with Erlin2**

201 Membralin is a novel protein with no conserved domains. RT-PCR analysis showed that
202 membralin mRNA was expressed in multiple tissues, including brain and spinal cord,
203 but not heart, skeletal muscle, or spleen (**Figure 4A**). Western blot analysis of spinal
204 cord samples from WT and KO mice showed specific expression of membralin in the
205 ER, but not in the cytosol or mitochondria (**Figure 4B**). Since our anti-membralin
206 antibody proved ineffective for immunostaining, we made a fusion protein by adding a
207 myc tag to the C-terminus of membralin (membralin-myc). Immunocytochemistry
208 demonstrated that membralin-myc co-localized with an ER marker, protein disulfide

isomerase (PDI), but not with markers for Golgi or mitochondria (**Figure 4C**). Membralin-myc was not expressed on the cell surface, since it was not detected in transfected cells without first permeabilizing the membrane (data not shown). Software for topology prediction from the Center for Biological Sequences (CBS, TMHMM) indicated that membralin is most likely a transmembrane protein with 4-6 membrane-spanning regions, containing an ER-lumen domain between membrane-spanning regions 1 and 2. Additionally, the protein has multiple glycosylation sites and cytosolic regions at both the N- and C-terminal ends (**Figure 4- figure supplement 1A,B**). These data suggest that membralin is a membrane protein most likely localized to the ER and/or outer nuclear envelope.

A recent study defining human ER-associated degradation (ERAD) networks through an integrative mapping strategy identified a potential interaction of membralin (C19orf6) with Erlin2 (Christianson et al., 2012). Erlin2 is a protein that is enriched in ER lipid rafts (Browman et al., 2006; Ikegawa et al., 1999), and mutations in Erlin2 have been linked to several human diseases with motor dysfunction (Al-Saif et al., 2012; Al-Yahyaee et al., 2006; Alazami et al., 2011; Wakil et al., 2013; Yildirim et al., 2011). We designed experiments to verify the membralin/Erlin2 interaction. We found that GFP-tagged membralin not only co-localized with but also manifested a strong FRET signal with mCherry-tagged Erlin2 in the ER (**Figure 5A**). The FRET efficiency was significantly higher for GFP-tagged membralin and mCherry-tagged Erlin2 (18.00 ± 0.70%) than the negative control (GFP and mCherry, 0.15 ± 0.05%), consistent with a direct interaction of the two molecules (**Figure 5B**). Additionally, Myc-tagged full-length membralin co-immunoprecipitated with HA-tagged Erlin2 (**Figure 5C**). This interaction

of membralin with Erlin2 further supports the notion that membralin is an ER membrane protein, and also suggests that loss of membralin could potentially increase ER stress by interrupting ERAD. Indeed, we found that the ER membrane protein, CD3-δ, was cleared more slowly in mouse embryonic fibroblasts (MEFs) prepared from membralin KO mice than from wild-type mice (**Figure 5D**), whereas there was no change in the clearance of the ER lumenal protein, NHK (**Figure 5- figure supplement 1**). These results suggest that membralin deficiency affects degradation of ER membrane proteins, which could potentially increase ER stress. Thus, we next analyzed ER stress in membralin KO mice.

Increased ER stress in membralin KO mice

Increased ER stress is thought to be involved in some forms of motor neuron disease, including ALS (Atkin et al., 2006; Kanekura et al., 2009; Nagata et al., 2007; Nishitoh et al., 2008; Saxena et al., 2009). We therefore tested whether the absence of membralin impacted ER stress (Walter and Ron, 2011). Western blot analysis showed that the levels of GRP78 and ATF4, two molecules induced during ER stress via activation of the PERK signaling pathway, were consistently higher in the spinal cord of P3 membralin KO mice than WT mice (154 ± 35% and 412 ± 39% of WT, respectively; KO, n = 4; WT, n = 3; **Figure 6A**). In contrast, levels of spliced XBP-1, indicating activation of the IRE1 signaling pathway during ER stress, were not altered (**Figure 6- figure supplement 1A**). Furthermore, tunicamycin, an inducer of ER stress, produced a greater degree of cell death in mouse embryonic fibroblasts (MEFs) from KO mice than from WT mice (**Figure 6B**). Tunicamycin exposure also increased CHOP and ATF4 levels earlier and to a greater extent in MEFs from KO mice; GRP78 levels were also

higher at 24 h post-exposure (**Figure 6C**). Basal levels of ATF4, but not CHOP, were higher in membralin KO mice than WT mice (**Figure 6C**), but XBP-1 splicing was not altered (**Figure 6- figure supplement 1B**). Collectively, these data suggest that loss of membralin increases basal ER stress and makes cells more vulnerable to additional ER stress-induced injury.

Discussion

HMN is usually subdivided into two groups: proximal HMN, i.e., classical spinal muscular atrophy (SMA) syndromes, and distal HMN, which clinically resemble Charcot-Marie-Tooth (CMT) syndromes without obvious sensory abnormalities. In contrast to proximal HMN, distal HMN represents a heterogeneous group of peripheral neuropathies affecting mainly distal muscles with both autosomal dominant and recessive inheritance (Irobi et al., 2004; Irobi et al., 2006; Irobi-Devolder, 2008). Seven subgroups of distal HMN were initially proposed based on age of onset, mode of inheritance, and clinical features of a limited number of affected families (Harding, 1993). Additional forms of distal HMN were subsequently reported, adding more genetic complexity. A dozen causal gene loci and other associated genes have been identified for distal HMN (exclusive of type I); these genes encode for a functionally heterogeneous group of proteins, as summarized in recent reviews (Irobi et al., 2004; Irobi et al., 2006; Irobi-Devolder, 2008). The biological functions of the affected proteins include stress responses (small heat shock proteins HSP22, HSP27), housekeeping (GARS, glycyl tRNA synthetase), protein glycosylation in the ER (seipin), RNA

processing (immunoglobulin μ-binding protein 2 [LGHMBP2] and senataxin), and axonal transport (dynactin). It is not clear, however, how these mutated proteins of diverse cellular function converge to affect motor neuron survival selectively. In fact, their expression is not even restricted to motor neurons. A similar case is found for membralin in this study. Therefore, further studies on molecular mechanisms underlying the selectivity of motor neuron death in distal HMN will be critical to understanding the disease. A hint towards pathogenesis may be found in prior work in conjunction with our new findings and involves an unusual susceptibility of motor neurons to various forms of cell stress, particularly ER stress.

Accordingly, the membralin KO mouse generated in our laboratory provides a good model to study selective motor neuron vulnerability. These mice display severe motor neuron loss and muscle wasting, leading to paresis and death. Although the early disease onset in membralin KO mice is similar to that seen in an SMA mouse model (Hsieh-Li et al., 2000; Monani et al., 2000), the pattern of motor neuron injury in membralin KO mice is reminiscent of human distal HMN rather than proximal HMN, as observed in SMA. Of the dozen known causal genes for distal HMN, only a few show autosomal recessive inheritance, and no mouse model has heretofore been generated (Irobi et al., 2004; Irobi et al., 2006; Irobi-Devolder, 2008). Therefore, the membralin null mouse represents a novel model for human distal HMN. Additionally, our studies demonstrate the previously unknown function of membralin in motor neuron survival. Our findings from endogenous and heterologous expression studies suggest that membralin is mainly located in the ER. Relatively low expression of membralin seems sufficient for normal function, as heterozygotes of the membralin KO survived, and

transgene rescue of the membralin KO did not require high expression levels. Importantly, in our rescue experiments membralin transgene expression was primarily in brain, not muscle, consistent with the notion that the pathogenic process is predominantly neural in origin. The exact mechanisms underlying motor neuron death in membralin KO mice are not yet clear, although death occurs very rapidly at an early and well-defined postnatal stage. Thus, membralin KO mice can be used not only as an early-onset model of motor neuron disease but also to determine if there are features in common with late-onset motor neuron disease, such as motor neuron-specific vulnerability to ER stress (Roselli and Caroni, 2015; Saxena et al., 2009), dying back axonopathy (Fischer et al., 2004;Coleman, 2005), or non-cell autonomous death (Boillee et al., 2006; Kang et al., 2013; Yamanaka et al., 2008).

Previously, membralin was predicted to encode a transmembrane protein, but it lacked homology with any known protein domains and was not known to interact with other membrane proteins (Andersson and von Euler, 2002). In the present study, we found that membralin interacts with Erlin2, an ER membrane protein potentially involved in ERAD (Christianson et al., 2012). The exact cellular functions of Erlin2 are not clear, although it has been reported to interact with several ER resident E3 ligases such as GP78 and Hrd1 that are important for ERAD (Christianson et al., 2012). Additionally, Erlin2 has been shown to regulate ER membrane proteins such as Inositol 1,4,5-trisphosphate receptors (Pearce et al., 2007). It is conceivable that membralin assists Erlin2 in a complex that retrotranslocates unfolded proteins from the ER lumen to the cytosol, thus facilitating their ubiquitination for degradation (Brodsky, 2012; Carvalho et al., 2006; Carvalho et al., 2010; Denic et al., 2006; Schulze et al., 2005; Smith et al.,

2011; Vembar and Brodsky, 2008). Consequently, membralin deficiency might increase both basal ER stress and vulnerability to ER stress-induced cell death, and this is exactly what we observed. We also found differences in Isg15 levels in membralin KO mice, leading to ISGylation, a process that represents a type I interferon-dependent, ER stress-triggered event. This observation is interesting in light of prior findings showing that ISGylation is a pre-symptomatic event observed in a mouse model of ALS (Wang et al., 2011). Collectively, our data suggest that loss of membralin may contribute to degeneration by increasing ER stress in motor neurons, which are especially vulnerable to such stress due to their large metabolic demand. This demand is particularly prevalent postnatally when maturation of motor neurons requires synthesis of proteins for production of dendritic trees, synaptic connections, and ionic conductances (Carrascal et al., 2005; Li et al., 2005; Vinay et al., 2000).

Additionally, disruption of ER-associated degradation (ERAD) in SOD1 mutant mice is known to induce ER stress, activation of apoptosis signal-regulating kinase1 (ASK1), and motor neuron cell death (Nishitoh et al., 2008). Mutations in Erlin2 have been linked to human disease, including intellectual disability, motor dysfunction, hereditary spastic paraplegia, and juvenile primary lateral sclerosis (Al-Saif et al., 2012; Al-Yahyaee et al., 2006, 2006 #264; Alazami et al., 2011; Wakil et al., 2013; Yildirim et al., 2011). Moreover, disturbance in various other components of ERAD, including OS-9, erasin, ubiquilin2, torsinA, and Derlin1, cause ER stress (Alcock and Swanton, 2009; Deng et al., 2011; Lim et al., 2009; Nery et al., 2011; Nishitoh et al., 2008), and some of these genes have been linked to ALS (Al-Saif et al., 2012; Alazami et al., 2011; Alcock and Swanton, 2009; Lim et al., 2009; Nery et al., 2011; Nishitoh et al., 2008; Wakil et al.,

2013; Yildirim et al., 2011). Therefore, future elucidation of the exact role of membralin in ERAD will undoubtedly be important for understanding the contribution of ER stress to motor neuron diseases. Interestingly, there are more than 50 single nucleotide polymorphisms (SNPs) in the coding region of human membralin that result in missense mutations (NBCI SNP database). The minor allele frequency (MAP) of most SNPs is either low or has not been determined, suggesting that these SNPs are not common in the human population. Thus, our studies point to a specific role of membralin in motor neuron survival and potentially open a new avenue for research in the field of human motor neuron diseases.

Methods

Constructing a target vector

We used the 3.6 kb (Apa I/Spe I) and 3.2 kb (BamH I/Kpn I) DNA fragments flanking the target region as the 5'- and 3'-arms, respectively, for the ~11.4 kb pGTN29/ GluN3B /membralin targeting vector (see Supplementary Figure 1a). Homologous recombination generated a ~5 kb size difference between the original and recombinant genes, facilitating their analysis. During construction of the targeting vector, one SpeI site at the junction of the 5'-arm and the target region was eliminated and another SpeI site was introduced at the junction of the target region and 3'-arm. These restriction site variations allowed us to designed a 3' probe, a 436 bp fragment from Xho I digestion, that hybridized to the 14 kb and 6 kb fragments generated by SpeI digestion or 9.1 kb and 8.4 kb fragments generated by EcoR I digestion (see **Figure 1-figure supplement 1A,B**) from the WT and recombinant alleles, respectively.

Generation of an ES cell line and GluN3B/membralin double knockout (DKO) mice

All described procedures for animal were approved by the Institutional Animal Care and Use Committee of Sanford-Burnham Medical Research Institute and conducted in compliance with the Guide for the Care and Use of Laboratory Animals. Both sexes of mice were used for experiments and maintained in an institute facility accredited by the Association for Assessment and Accreditation of Laboratory Animal Care (AAALAC). The C1 ES cells were cultured in the presence of leukemia inhibitor factor (LIF) on

primary embryo fibroblast feeder cells and were transfected with the linearized pGTN29/GluN3B /membralin target vector DNA by electroporation at 400 V, 25 mF. Thirty-six hours after transfection, 0.48 mg/ml G418 was added to select for cells that have acquired the Neo^r gene by homologous recombination with the targeting vector. The ES cells with the correct recombination were confirmed by standard Southern blot analysis using the probe described above. GluN3B/membralin-targeted ES cell lines were used for blastocyst injection. Then, 6 to 10 embryos, including 2 uninjected blastocysts as carriers, were transferred into one uterine horn of each pseudopregnant foster mother (F1 of DBA X C57BL/J6j). Chimeric mice were identified by eye pigmentation. Further breeding was made to test for germ line transmission of the injected ES cells. Mouse-tail DNA was used to identify homozygotes and heterozygotes by the same procedure used in testing ES cells. Once the DKO line was established, we also designed a PCR method to simplify genotyping using a pair of primers for the GluN3B sequence in WT alleles and a pair of primers for the Neo sequence in the DKO allele (see **Supplementary File 1**).

Generation of transgenic mouse lines carrying GluN3B and membralin transgenes

We have obtained the mouse full-length GluN3B cDNA clone from Dr. Yuzaki as a gift (Matsuda et al., 2002). A full-length mouse membralin cDNA clone (ID# 3813678) was purchased from distributors of the Integrated Molecular Analysis of Genomes and their Expression (I.M.A.G.E) consortium (http://image.llnl.gov/image/html/idistributors.shtml). We used the mouse GluN3B promoter that drives gene expression mainly in motor neurons from late embryonic stages to adult (database from NINDS Gensat Bac

Transgenic Project, http://www.gensat.org/index.html). In addition, we used the mouse prion promoter, which drives high transgene expression in mouse neurons (Baybutt and Manson, 1997; Gispert et al., 2003; Loftus et al., 2002), to express the transgene in a broader brain area. The selected full-length transgene was subcloned downstream of either promoter, followed by an internal ribosome entry site (IRES) or a sequence coding the GFP. The insert containing promoter, transgene, and IRES/GFP sequences was isolated by restriction digest followed by gel purification. The purified DNA fragments were injected into fertilized eggs to generate transgenic mice (C57BL/J6j) in our institute's Transgenic Facility according to established protocol. We used PCR methods to genotype transgenic mice using a pair of primers (see **Supplementary File 1**).

Rescue of DKO mice by GluN3B and membralin transgenes

Hemizygotes of transgenic mice were bred with DKO mice to obtain double heterozygotes [transgene$^{+/-}$/ (GluN3B/membralin)$^{+/-}$]. The double heterozygote was further bred to obtain mice that express the transgene in the GluN3B/membralin null background [transgene$^{+/-}$/(GluN3B /membralin)$^{-/-}$], and tested for GFP and transgene expression using RT-PCR. The crossed transgene/DKO mouse line was subjected to histological tests for examining motor neuron integrity. The survival time of the [transgene$^{+/-}$/(GluN3B/membralin)$^{-/-}$] mice were monitored and compared with that of DKO mice to determine the ability of the transgene to rescue the DKO mice phenotype.

Generation of membralin KO mice by a gene trapping method

We generated membralin KO mice by using ES cells (gift of Sanger Institute) with a disrupted membralin gene by a gene trapping method (Brennan and Skarnes, 1999; Skarnes et al., 2004). Briefly, a trapping vector containing an RNA splicing acceptor sequence was inserted between exon 1 and 2 of the membralin gene in ES cells to disrupt normal RNA splicing. The positive ES cell clone was confirmed by sequencing and used for blastocyst injection to generate membralin knockout (KO) mice (C57BL/J6j). RT-PCR experiments using primers from exon 1 and 2 further confirmed that homozygote mice carrying membralin/trapping vector alleles did not express membralin mRNAs with sequences beyond exon 2.

Immunostaining and histological analysis

Previously established protocols were used for staining spinal cord sections or cultured cells (Xing et al., 2006), with the following antibodies: mouse anti-GFAP (Sigma-Aldrich), rabbit anti-IBA-1 (Wako Chemicals USA, Inc.), and anti-Hb9 (a gift from Dr. Pfaff), followed by incubation with either a fluorophore-attached or a biotinylated secondary antibody (Life Technologies and Vector Laboratories). Immunosignals were detected either directly under epifluorescence microscopy, or after using a Vectastain Elite ABC kit (Vector Laboratories) with 3,3'-diaminobenzidine (DAB) visualization (Roche Applied Science). The number of motor neurons in layers VIII and IX of the lumbar spinal cord were counted using stereological methods in WT, DKO, and membralin KO mice (Coggeshall and Lekan, 1996). Briefly, consecutive sections (12 μm in thickness) of the lumber enlargement (L1-L5) were collected for immunostaining with anti-Hb9 antibody to identify motor neurons. The number of motor neurons in each

section was counted stereologically using adjacent sections for reference and look-up (physical disector). The total number of motor neurons was obtained for each mouse, and the mean value for 3 mice at each age group was calculated and normalized to that of WT mice. The general appearance of motor neurons was examined by conventional staining methods used in analysis of SOD1 mutant mice, including hematoxylin/eosin and cresyl violet staining.

HEK 293 cells were used for investigating the subcellular localization of membralin. A membralin-myc fusion protein was constructed by tagging the C-terminal of membralin with a Myc sequence using the pcDNA3.1(-) Myc/his vector (Invitrogen). HEK 293 cells were plated onto coverslips, transfected with the membralin-Myc overnight, and fixed 48 h after transfection with 4% PFA with 0.5% Triton X-100 in PBS. After blocking with 10% normal goat serum in PBS for 60 min, the cells were double stained by anti-Myc rabbit polyclonal antibody (Sigma) for membralin-Myc detection, followed by Alexa fluor®-conjugated secondary antibodies (Invitrogen). Subcellular organelles were stained by either anti-PDI antibody (Enzo Life Science) for ER labeling, anti-GMP130 antibody (BD bioscience) for Golgi labeling, or anti-mitochondria antibody (113-1, Abcam) for mitochondrial labeling, followed by Alexa fluor®-conjugated secondary antibodies (Invitrogen). DAPI was used to stain nuclei. Images were captured under confocal microscopy (Zeiss 710).

Electron microscopy

Dorsal and ventral roots of lumbar segments (L3-L5) of the spinal cord were dissected out from P5 WT and DKO mice. Samples were immediately placed in 4%

paraformaldehyde plus 1% glutaraldehyde in 0.1 M phosphate buffer and simultaneously processed for electron microscopy as described previously (Liu et al., 1998). Briefly, samples were osmicated in 1% OsO_4 for 10-20 min followed by washing in 0.1 M phosphate buffer and then dehydrated in graded ethanol and 100% acetone. Each sample was oriented and placed in a Flat Embedding Mold (Ted Pella, Redding, CA) filled with Araldite (EMS, Fort Washington, PA). Embedded dorsal or ventral roots of different genotypes were dissected and the cross sections of the roots were re-cut on an ultramicrotome (Ultracut, Leica) at 70-80nm. Serial thin sections were collected on Formva-coated single slot nickel grids and stained with uranyl acetate and lead citrate. Ultrathin sections were examined in a Philips CM120 electron microscope at 80 KV. Digitized images were acquired by a high-resolution (2K X 2K) CCD camera (Gatan, Inc., Pleasanton, CA), processed using software provided by the manufacturer (DigitalMicrograph), and displayed with Photoshop CS (Adobe Systems, San Jose, CA).

Northern blot analysis

Two DNA fragments were purified by enzymatic digestion of membralin cDNA using BamH I/Bgl II and Not I/BamH I, respectively, to generate two probes specific to regions of exon VII-X and the last exon (XI) of membralin. Northern blot analysis was performed using these two probes labeled with ^{32}P by random priming. Ten μg of total mouse RNA per lane were analyzed by electrophoresis on a 1.1% denaturing gel and subsequently transferred to a nylon membrane. The blot was hybridized at 42 °C in a solution containing 50% formamide, 6x SSC, 5x Denhardt's reagent and 0.5% SDS. The blots were dried and exposed to autoradiographic films for analysis.

Analysis of the interaction between membralin and Erlin2

cDNAs for mouse membralin and Erlin2 were purchased from distributors of the Integrated Molecular Analysis of Genomes and their Expression (I.M.A.G.E) consortium (http://image.llnl.gov/image/html/idistributors.shtml) and subcloned into a pcDNA3.1 vector for mammalian cell expression. C-terminal tagged membralin (membralin-myc or membralin-mCherry) and N-terminal or C-terminal tagged Erlin2 (Erlin2-EGFP or Erlin2-HA) and N-terminal or C-terminal tagged Erlin2 (Erlin2-EGFP or Erlin2-HA) were constructed by introducing corresponding tag fragments generated by the PCR method, and all constructs were confirmed by sequencing. Membralin-myc and Erlin2-HA were co-transfected in HEK 293 cells and total cell lysates collected 48 h after transfection for co-immunoprecipitation-immunoblot assay.

The interaction of Erlin2-EGFP and membralin-mCherry was validated by the acceptor photobleaching method for FRET detection (Karpova and McNally, 2006). Briefly, HEK 293 cells were transfected with Erlin2-EGFP and membralin-mCherry for 24 h. A Zeiss 710 NLO microscope (Carl Zeiss Inc.) was used to record the fluorescence of EGFP and mCherry in transfected cells. Three pre-bleached and five post-bleached images were acquired. Averaged fluorescence intensities of the donor were calculated from the measurement of regions of interest for each experimental set before and after bleaching. The efficiency of FRET was calculated by $E_{fret} = 1 - (I_a/I_b)$, where I_a and I_b represent the steady-state donor fluorescence in the presence and the absence of the acceptor, respectively. Seven Ala-linked EGFP-mCherry plasmids were

517 transfected into HEK 293 cells and were used as a positive FRET control (FRET
518 efficiency = ~50%, data not shown). FRET efficiencies were reported as mean ± s.e.m.
519
520 **Assays for detecting alterations in ER stress signaling pathways**
521 We measured levels of GRP78, CHOP, and ATF4, components of three canonical
522 branches of unfolded protein responses (UPR), by Western blot analysis using the
523 spinal cord tissues and MEFs from membralin KO mice and WT littermates. The
524 antibodies against these proteins were purchased from commercial sources: GRP78
525 (H-129, 1:1000; Santa Cruz Biotechnology), CHOP (2895S, 1:1000; Cell Signaling), and
526 ATF4 (SC200, 1:500; Santa Cruz Biotechnology). Total RNA was isolated from the
527 spinal cord of membralin mutant mice and WT littermate using TRIzol reagent
528 (Invitrogen). The following set of primers was used to detect the expression of mouse
529 Xbp-1 (GATCCTGACGAGGGTCCAAGA and ACAGGGTCCAACTTGTCCAG).
530
531 **Toxicity assay *in vitro***
532 MEFs from membralin KO mice and WT littermates were isolated from day 12.5
533 embryos and cultured by conventional methods. In the toxicity assay, the percentage of
534 cell death was measured by counting cells or using the CellTiter 96 Aqueous Non-
535 Radioactive Cell Proliferation Assay kit (Promega) after MEF cells were exposed to the
536 ER stress inducer, tunicamycin, for 24 h.
537
538 **Statistical analysis**

The sample size was 3–10 per genotype for animal histology and 3–6 for protein or transcript expression as well as for cell viability studies, as determined by Power Analyses of previous data. The experiments were not randomized. Although the initial investigator performing the experiments was not blinded, the samples and animal results were then examined by a group of the investigators masked to experimental identity in order to evaluate the results. All data points demonstrated a normal distribution and were all included in the analysis. Data are presented as mean ± s.e.m. and analyzed by a Student's *t*-test for pairwise comparisons. Statistical analyses were conducted using GraphPad Prism software (version 6). A P value < 0.05 was considered statistically significant.

Acknowledgments

We thank M. Yuzaki at Keio University for the mouse full-length GluN3B cDNA clone and A. Aguzzi at University Hospital of Zurich for the mouse prion promoter. We thank Wellcome Trust Sanger Institute for providing ES cells carrying membralin deletion mutant gene by trapping method. We thank the animal facility at the Sanford-Burnham Medical Research institute for generating and maintaining mutant mouse lines. We thank Yeast Model Systems Genomics at Duke University for service of Yeast two-hybrid screening. This work was supported in part by NIH grants to S.A.L (P01 HD29587, R01 NS086890, and P30 NS076411) and D.Z (R01 NS043434).

Author Contributions

B.Y. and M.Q. designed and performed most experiments, analyzed the data, and wrote the paper. R.W. performed histological experiments of DKO mice. J.E.C. designed and conducted experiments in generating the DKO mouse line. X.L. performed EM studies. B.Z. performed FRET experiments. S.N. and J.L.M. provided experimental assistance in generating the DKO mouse line. N.N. provided guidance for experimental design and edited the manuscript. K.J.S provided clinical insight and edited paper. S.A.L provided guidance for experimental design and helped write the manuscript. D.Z. conceived of, designed, and supervised the *in vivo* and *in vitro* experiments, and wrote the manuscript.

Competing financial interests

The authors declare no competing financial interests.

References

1. Al-Saif, A, Bohlega, S & Al-Mohanna, F. Loss of ERLIN2 function leads to juvenile primary lateral sclerosis. Annals of neurology 72: 510-516, 2012
2. Al-Yahyaee, S, Al-Gazali, LI, De Jonghe, P, Al-Barwany, H, Al-Kindi, M, De Vriendt, E, Chand, P, Koul, R, Jacob, PC, Gururaj, A, Sztriha, L, Parrado, A, Van Broeckhoven, C & Bayoumi, RA. A novel locus for hereditary spastic paraplegia with thin corpus callosum and epilepsy. Neurology 66: 1230-1234, 2006
3. Alazami, AM, Adly, N, Al Dhalaan, H & Alkuraya, FS. A nullimorphic ERLIN2 mutation defines a complicated hereditary spastic paraplegia locus (SPG18). Neurogenetics 12: 333-336, 2011

4. Alcock, F & Swanton, E. Mammalian OS-9 is upregulated in response to endoplasmic reticulum stress and facilitates ubiquitination of misfolded glycoproteins. Journal of Molecular Biology 385: 1032-1042, 2009

5. Andersson, O & von Euler, G. Characterization and expression of the gene encoding membralin, an evolutionary conserved protein expressed in the central nervous system. Brain Research - Gene Expression Patterns 1: 205-212, 2002

6. Atkin, JD, Farg, MA, Turner, BJ, Tomas, D, Lysaght, JA, Nunan, J, Rembach, A, Nagley, P, Beart, PM, Cheema, SS & Horne, MK. Induction of the unfolded protein response in familial amyotrophic lateral sclerosis and association of protein-disulfide isomerase with superoxide dismutase 1. Journal of Biological Chemistry 281: 30152-30165, 2006

7. Atkin, JD, Farg, MA, Walker, AK, McLean, C, Tomas, D & Horne, MK. Endoplasmic reticulum stress and induction of the unfolded protein response in human sporadic amyotrophic lateral sclerosis. Neurobiology of Disease 30: 400-407, 2008

8. Baybutt, H & Manson, J. Characterisation of two promoters for prion protein (PrP) gene expression in neuronal cells. Gene 184: 125-131, 1997

9. Boillee, S, Yamanaka, K, Lobsiger, CS, Copeland, NG, Jenkins, NA, Kassiotis, G, Kollias, G & Cleveland, DW. Onset and Progression in Inherited ALS Determined by Motor Neurons and Microglia. Science 312: 1389-1392, 2006

10. Brennan, J & Skarnes, WC. Gene trapping in mouse embryonic stem cells. Methods in Molecular Biology 97: 123-138, 1999

11. Brodsky, JL. Cleaning up: ER-associated degradation to the rescue. Cell 151: 1163-1167, 2012

12. Browman, DT, Resek, ME, Zajchowski, LD & Robbins, SM. Erlin-1 and erlin-2 are novel members of the prohibitin family of proteins that define lipid-raft-like domains of the ER. Journal of Cell Science 119: 3149-3160, 2006

13. Carrascal, L, Nieto-Gonzalez, JL, Cameron, WE, Torres, B & Nunez-Abades, PA. Changes during the postnatal development in physiological and anatomical characteristics of rat motoneurons studied in vitro. Brain Research - Brain Research Reviews 49: 377-387, 2005

14. Carvalho, P, Goder, V & Rapoport, TA. Distinct ubiquitin-ligase complexes define convergent pathways for the degradation of ER proteins. Cell 126: 361-373, 2006

15. Carvalho, P, Stanley, AM & Rapoport, TA. Retrotranslocation of a misfolded luminal ER protein by the ubiquitin-ligase Hrd1p. Cell 143: 579-591, 2010

16. Chatterton, JE, Awobuluyi, M, Premkumar, LS, Takahashi, H, Talantova, M, Shin, Y, Cui, J, Tu, S, Sevarino, KA, Nakanishi, N, Tong, G, Lipton, SA & Zhang, D. Excitatory glycine receptors containing the NR3 family of NMDA receptor subunits. Nature 415: 793-798, 2002

17. Chen, YC, Davidson, B, Cheng, CC, Maitra, A, Giuntoli, RL, 2nd, Hruban, RH, Wang, TL & Shih Ie, M. Identification and characterization of membralin, a novel tumor-associated gene, in ovarian carcinoma. Biochimica et Biophysica Acta 1730: 96-102, 2005

18. Christianson, JC, Olzmann, JA, Shaler, TA, Sowa, ME, Bennett, EJ, Richter, CM, Tyler, RE, Greenblatt, EJ, Harper, JW & Kopito, RR. Defining human ERAD networks through an integrative mapping strategy. Nature Cell Biology 14: 93-105, 2012

19. Coggeshall, RE & Lekan, HA. Methods for determining numbers of cells and synapses: a case for more uniform standards of review. Journal of Comparative Neurology 364: 6-15, 1996

20. Coleman, M. Axon degeneration mechanisms: commonality amid diversity. Nature Reviews Neuroscience 6: 889-898, 2005

21. Das, I, Krzyzosiak, A, Schneider, K, Wrabetz, L, D'Antonio, M, Barry, N, Sigurdardottir, A & Bertolotti, A. Preventing proteostasis diseases by selective inhibition of a phosphatase regulatory subunit. Science 348: 239-242, 2015

22. Deng, H-X, Chen, W, Hong, S-T, Boycott, KM, Gorrie, GH, Siddique, N, Yang, Y, Fecto, F, Shi, Y, Zhai, H, Jiang, H, Hirano, M, Rampersaud, E, Jansen, GH, Donkervoort, S, Bigio, EH, Brooks, BR, Ajroud, K, Sufit, RL, Haines, JL, Mugnaini, E, Pericak-Vance, MA & Siddique, T. Mutations in UBQLN2 cause dominant X-linked juvenile and adult-onset ALS and ALS/dementia. Nature 477: 211-215, 2011

23. Denic, V, Quan, EM & Weissman, JS. A luminal surveillance complex that selects misfolded glycoproteins for ER-associated degradation. Cell 126: 349-359, 2006

24. Filezac de L'Etang, A, Maharjan, N, Cordeiro Brana, M, Ruegsegger, C, Rehmann, R, Goswami, A, Roos, A, Troost, D, Schneider, BL, Weis, J & Saxena,

S. Marinesco-Sjogren syndrome protein SIL1 regulates motor neuron subtype-selective ER stress in ALS. Nature Neuroscience 18: 227-238, 2015

25. Fischer, LR, Culver, DG, Tennant, P, Davis, AA, Wang, M, Castellano-Sanchez, A, Khan, J, Polak, MA & Glass, JD. Amyotrophic lateral sclerosis is a distal axonopathy: evidence in mice and man. Experimental Neurology 185: 232-240, 2004

26. Gispert, S, Del Turco, D, Garrett, L, Chen, A, Bernard, DJ, Hamm-Clement, J, Korf, HW, Deller, T, Braak, H, Auburger, G & Nussbaum, RL. Transgenic mice expressing mutant A53T human alpha-synuclein show neuronal dysfunction in the absence of aggregate formation. Molecular and Cellular Neuroscience 24: 419-429, 2003

27. Harding, A. Inherited neuronal atrophy and degeneration predominantly of lower motor neurons. in *Peripheral Neuropathy* (eds. Dyck, PJ, Thomas, PK, Griffin J. W., Low P. A. & F., PJ) 1051-1064 (W.B Saunders Company, Philadephia, 1993).

28. Hetz, C & Mollereau, B. Disturbance of endoplasmic reticulum proteostasis in neurodegenerative diseases. Nature Reviews Neuroscience 15: 233-249, 2014

29. Hsieh-Li, HM, Chang, JG, Jong, YJ, Wu, MH, Wang, NM, Tsai, CH & Li, H. A mouse model for spinal muscular atrophy. Nature Genetics 24: 66-70, 2000

30. Ikegawa, S, Isomura, M, Koshizuka, Y & Nakamura, Y. Cloning and characterization of a novel gene (C8orf2), a human representative of a novel gene family with homology to C. elegans C42.C1.9. Cytogenetics and Cell Genetics 85: 227-231, 1999

31. Irobi, J, De Jonghe, P & Timmerman, V. Molecular genetics of distal hereditary motor neuropathies. Human Molecular Genetics 13 Spec No 2: R195-202, 2004
32. Irobi, J, Dierick, I, Jordanova, A, Claeys, KG, De Jonghe, P & Timmerman, V. Unraveling the genetics of distal hereditary motor neuronopathies. Neuromolecular Medicine 8: 131-146, 2006
33. Irobi-Devolder, J. A molecular genetic update of inherited distal motor neuropathies. Verhandelingen Koninklijke Academie voor Geneeskunde van België 70: 25-46, 2008
34. Ito, Y, Yamada, M, Tanaka, H, Aida, K, Tsuruma, K, Shimazawa, M, Hozumi, I, Inuzuka, T, Takahashi, H & Hara, H. Involvement of CHOP, an ER-stress apoptotic mediator, in both human sporadic ALS and ALS model mice. Neurobiology of Disease 36: 470-476, 2009
35. Jiang, HQ, Ren, M, Jiang, HZ, Wang, J, Zhang, J, Yin, X, Wang, SY, Qi, Y, Wang, XD & Feng, HL. Guanabenz delays the onset of disease symptoms, extends lifespan, improves motor performance and attenuates motor neuron loss in the SOD1 G93A mouse model of amyotrophic lateral sclerosis. Neuroscience 277C: 132-138, 2014
36. Kanekura, K, Suzuki, H, Aiso, S & Matsuoka, M. ER stress and unfolded protein response in amyotrophic lateral sclerosis. Molecular Neurobiology 39: 81-89, 2009
37. Kang, SH, Li, Y, Fukaya, M, Lorenzini, I, Cleveland, DW, Ostrow, LW, Rothstein, JD & Bergles, DE. Degeneration and impaired regeneration of gray matter

oligodendrocytes in amyotrophic lateral sclerosis. Nature Neuroscience 16: 571-579, 2013

38. Karpova, T & McNally, JG. Detecting protein-protein interactions with CFP-YFP FRET by acceptor photobleaching. Current protocols in cytometry / editorial board, J. Paul Robinson, managing editor. Chapter 12: Unit12 17, 2006

39. Kikuchi, H, Almer, G, Yamashita, S, Guegan, C, Nagai, M, Xu, Z, Sosunov, AA, McKhann, GM, 2nd & Przedborski, S. Spinal cord endoplasmic reticulum stress associated with a microsomal accumulation of mutant superoxide dismutase-1 in an ALS model. Proceedings of National Academy of Sciences (USA) 103: 6025-6030, 2006

40. Kim, I, Xu, W & Reed, JC. Cell death and endoplasmic reticulum stress: disease relevance and therapeutic opportunities. Nature Reviews Drug Discovery 7: 1013-1030, 2008

41. Lance-Jones, C. Motoneuron cell death in the developing lumbar spinal cord of the mouse. Brain Research 256: 473-479, 1982

42. Li, Y, Brewer, D, Burke, RE & Ascoli, GA. Developmental changes in spinal motoneuron dendrites in neonatal mice. Journal of Comparative Neurology 483: 304-317, 2005

43. Lim, PJ, Danner, R, Liang, J, Doong, H, Harman, C, Srinivasan, D, Rothenberg, C, Wang, H, Ye, Y, Fang, S & Monteiro, MJ. Ubiquilin and p97/VCP bind erasin, forming a complex involved in ERAD. The Journal of Cell Biology 187: 201-217, 2009

719 44. Lin, JH, Walter, P & Yen, TS. Endoplasmic reticulum stress in disease
720 pathogenesis. Annual Review of Pathology 3: 399-425, 2008
721 45. Lindholm, D, Wootz, H & Korhonen, L. ER stress and neurodegenerative
722 diseases. Cell Death and Differentiation 13: 385-392, 2006
723 46. Liu, XB, Munoz, A & Jones, EG. Changes in subcellular localization of
724 metabotropic glutamate receptor subtypes during postnatal development of
725 mouse thalamus. Journal of Comparative Neurology 395: 450-465, 1998
726 47. Loftus, SK, Erickson, RP, Walkley, SU, Bryant, MA, Incao, A, Heidenreich, RA &
727 Pavan, WJ. Rescue of neurodegeneration in Niemann-Pick C mice by a prion-
728 promoter-driven Npc1 cDNA transgene. Human Molecular Genetics 11: 3107-
729 3114, 2002
730 48. Matsuda, K, Kamiya, Y, Matsuda, S & Yuzaki, M. Cloning and characterization of
731 a novel NMDA receptor subunit NR3B: a dominant subunit that reduces calcium
732 permeability. Brain Research - Molecular Brain Research 100: 43-52, 2002
733 49. Monani, UR, Sendtner, M, Coovert, DD, Parsons, DW, Andreassi, C, Le, TT,
734 Jablonka, S, Schrank, B, Rossol, W, Prior, TW, Morris, GE & Burghes, AH. The
735 human centromeric survival motor neuron gene (SMN2) rescues embryonic
736 lethality in Smn(-/-) mice and results in a mouse with spinal muscular atrophy.
737 Human Molecular Genetics 9: 333-339, 2000
738 50. Nagata, T, Ilieva, H, Murakami, T, Shiote, M, Narai, H, Ohta, Y, Hayashi, T,
739 Shoji, M & Abe, K. Increased ER stress during motor neuron degeneration in a
740 transgenic mouse model of amyotrophic lateral sclerosis. Neurological Research
741 29: 767-771, 2007

51. Nery, FC, Armata, IA, Farley, JE, Cho, JA, Yaqub, U, Chen, P, da Hora, CC, Wang, Q, Tagaya, M, Klein, C, Tannous, B, Caldwell, KA, Caldwell, GA, Lencer, WI, Ye, Y & Breakefield, XO. TorsinA participates in endoplasmic reticulum-associated degradation. Nature Communications 2: 393, 2011

52. Niemann, S, Kanki, H, Fukui, Y, Takao, K, Fukaya, M, Hynynen, MN, Churchill, MJ, Shefner, JM, Bronson, RT, Brown, RH, Jr., Watanabe, M, Miyakawa, T, Itohara, S & Hayashi, Y. Genetic ablation of NMDA receptor subunit NR3B in mouse reveals motoneuronal and nonmotoneuronal phenotypes. European Journal of Neuroscience 26: 1407-1420, 2007

53. Nishi, M, Hinds, H, Lu, HP, Kawata, M & Hayashi, Y. Motoneuron-specific expression of NR3B, a novel NMDA-type glutamate receptor subunit that works in a dominant-negative manner. Journal of Neuroscience 21: RC185, 2001

54. Nishitoh, H, Kadowaki, H, Nagai, A, Maruyama, T, Yokota, T, Fukutomi, H, Noguchi, T, Matsuzawa, A, Takeda, K & Ichijo, H. ALS-linked mutant SOD1 induces ER stress- and ASK1-dependent motor neuron death by targeting Derlin-1. Genes & Development 22: 1451-1464, 2008

55. Pearce, MM, Wang, Y, Kelley, GG & Wojcikiewicz, RJ. SPFH2 mediates the endoplasmic reticulum-associated degradation of inositol 1,4,5-trisphosphate receptors and other substrates in mammalian cells. Journal of Biological Chemistry 282: 20104-20115, 2007

56. Roselli, F & Caroni, P. From Intrinsic Firing Properties to Selective Neuronal Vulnerability in Neurodegenerative Diseases. Neuron 85: 901-910, 2015

57. Saxena, S, Cabuy, E & Caroni, P. A role for motoneuron subtype-selective ER stress in disease manifestations of FALS mice. Nature Neuroscience 12: 627-636, 2009

58. Scheper, W & Hoozemans, JJ. Endoplasmic reticulum protein quality control in neurodegenerative disease: the good, the bad and the therapy. Current Medicinal Chemistry 16: 615-626, 2009

59. Schulze, A, Standera, S, Buerger, E, Kikkert, M, van Voorden, S, Wiertz, E, Koning, F, Kloetzel, PM & Seeger, M. The ubiquitin-domain protein HERP forms a complex with components of the endoplasmic reticulum associated degradation pathway. Journal of Molecular Biology 354: 1021-1027, 2005

60. Skarnes, WC, von Melchner, H, Wurst, W, Hicks, G, Nord, AS, Cox, T, Young, SG, Ruiz, P, Soriano, P, Tessier-Lavigne, M, Conklin, BR, Stanford, WL & Rossant, J. A public gene trap resource for mouse functional genomics. Nature Genetics 36: 543-544, 2004

61. Smith, MH, Ploegh, HL & Weissman, JS. Road to ruin: targeting proteins for degradation in the endoplasmic reticulum. Science 334: 1086-1090, 2011

62. Tobisawa, S, Hozumi, Y, Arawaka, S, Koyama, S, Wada, M, Nagai, M, Aoki, M, Itoyama, Y, Goto, K & Kato, T. Mutant SOD1 linked to familial amyotrophic lateral sclerosis, but not wild-type SOD1, induces ER stress in COS7 cells and transgenic mice. Biochemical and Biophysical Research Communications 303: 496-503, 2003

63. Vembar, SS & Brodsky, JL. One step at a time: endoplasmic reticulum-associated degradation. Nature Reviews Molecular Cell Biology 9: 944-957, 2008

64. Vinay, L, Brocard, F, Pflieger, JF, Simeoni-Alias, J & Clarac, F. Perinatal development of lumbar motoneurons and their inputs in the rat. Brain Research Bulletin 53: 635-647, 2000

65. Wakil, SM, Bohlega, S, Hagos, S, Baz, B, Al Dossari, H, Ramzan, K & Al-Hassnan, ZN. A novel splice site mutation in ERLIN2 causes hereditary spastic paraplegia in a Saudi family. European Journal of Medical Genetics 56: 43-45, 2013

66. Walker, AK, Farg, MA, Bye, CR, McLean, CA, Horne, MK & Atkin, JD. Protein disulphide isomerase protects against protein aggregation and is S-nitrosylated in amyotrophic lateral sclerosis. Brain 133: 105-116, 2010

67. Walter, P & Ron, D. The unfolded protein response: from stress pathway to homeostatic regulation. Science 334: 1081-1086, 2011

68. Wang, L, Popko, B, Tixier, E & Roos, RP. Guanabenz, which enhances the unfolded protein response, ameliorates mutant SOD1-induced amyotrophic lateral sclerosis. Neurobiology of Disease 71: 317-324, 2014

69. Wang, R, Yang, B & Zhang, D. Activation of interferon signaling pathways in spinal cord astrocytes from an ALS mouse model. Glia 59: 946-958, 2011

70. Xing, GG, Wang, R, Yang, B & Zhang, D. Postnatal switching of NMDA receptor subunits from NR2B to NR2A in rat facial motor neurons. European Journal of Neuroscience 24: 2987-2992, 2006

71. Yamanaka, K, Chun, SJ, Boillee, S, Fujimori-Tonou, N, Yamashita, H, Gutmann, DH, Takahashi, R, Misawa, H & Cleveland, DW. Astrocytes as determinants of disease progression in inherited amyotrophic lateral sclerosis. Nature Neuroscience 11: 251-253, 2008

72. Yildirim, Y, Orhan, EK, Iseri, SAU, Serdaroglu-Oflazer, P, Kara, B, Solakoglu, S & Tolun, A. A frameshift mutation of ERLIN2 in recessive intellectual disability, motor dysfunction and multiple joint contractures. Human Molecular Genetics 20: 1886-1892, 2011

Figure Legend

Figure 1.

Motor neuron death in GluN3B/Membralin double knockout (DKO) mice.

(**A**) DKO and wild-type (WT) littermate mice are shown at P5. The DKO mouse was unable to maintain correct posture. (**B**) Immunostaining with anti-Hb9 antibody revealed a dramatic decrease in the number of motor neurons in the lumbar spinal cord of DKO mice relative to WT littermate mice at P5 but not at P0. (**C**) The number of motor neurons in the lumbar spinal cord of KO and WT mice was not significantly different at P0 and P3. However, severe motor neuron loss was observed by P5 in DKO mice (n = 3) compared with WT mice (n = 3, *P < 0.05 by Student's t-test). (**D**) Glial fibrillary associated protein (GFAP) and ionized calcium-binding adapter molecule 1 (IBA-1) immunostaining in the spinal cord of WT and DKO mice. GFAP-positive astrocytes and IBA-1-positive microglial cells surrounding motor neurons (counter stained with Giemsa) of DKO mice showed swelling cell bodies and processes, a typical sign of astrogliosis. (**E,F)** Electron microscopic analysis of spinal roots showed that DKO mice at age P5 had severe damage of motor neuron axons in the ventral root (**E**) but not of sensory neuron axons in the dorsal root (**F**). Bar, 2 μm. (**G,H**) Damaged axons in the ventral root showed either vacuoles or loss of axoplasm (**G**), as an early sign of axonal damage. At a later stage of axonal damage, dark disintegrated myelin sheaths and amorphous lipid were present (**H**). Bar, 1 μm. (**I**) Percentage of injured axons in the ventral and dorsal roots of DKO and WT mice (*P < 0.05 by Student's t-test, n = 3). Data are mean ± s.e.m.

Figure 1- figure supplement 1

Generation of GluN3B/membralin double knockout (DKO) mice.

(**A)** GluN3B and membralin genes arranged in tail-to-tail fashion with overlapping 3' coding regions of both genes. Blue and brown boxes indicate predicted exons of GluN3B and membralin genes, respectively. The entire GluN3B coding region and part of the 3' coding region of membralin between the 5'- and 3'-arm (green arrows) in the WT allele was replaced by a Neo/PGK cassette in the DKO allele by homologous recombination. Spe I restriction sites, Southern blot and Northern blot probes, and primers used for PCR genotyping are indicated. (**B**) Genotyping by Southern blot analysis of SpeI-digested genomic DNA and by PCR. Mouse genomic DNA from 12 littermates from a single breeding pair of heterozygotes was subjected to Southern blot (*top panel*) and PCR analysis (*bottom panel*). Hybridizing bands or PCR fragments corresponding to WT and DKO allele are indicated. Both methods identified 4 WT (#6, 7, 8, and 10), 6 heterozygote (#1, 2, 3, 5, 9, and 12), and 2 homozygote (#4 and 11) mice. (**C**) Northern blot analysis of total RNA from null (KO) and WT mice using probes 1 and 2, derived from the last exon (XI) or exon VII-X of membralin, respectively (see **a**). Probe 1 generated a hybridization band (~2.8 kb) in WT but not in DKO mice. Probe 2 generated a ~2.8 kb band in WT and a ~3.4. kb band in DKO mice.

Figure 1- figure supplement 2

GluN3B/membralin double knockout (DKO) and WT mice show similar gross anatomy of the brain.

Left: Whole brains dissected from DKO and WT mice at P5. *Right*: Nissl-stained sagittal brain sections from DKO and WT mice at P5.

Figure 1- figure supplement 3

Expression of the motor neuron injury marker ISG15 in the spinal cord and brainstem of membralin KO mice.

(**A**) ISG15 immunosignal was barely detectable in spinal cord of P3 WT littermate mice but decorated the ventral grey matter (arrows) of cervical and lumbar (but not thoracic) spinal cord of membralin KO mice. By P5, stronger ISG15 immunostaining appeared in the ventral grey matter (arrows) at all levels of the spinal cord in KO mice. (**B**) Similarly, prominent ISG15 staining was observed at P5 in the facial nucleus (dotted circle) of KO but not WT littermate mice. Large motor neurons are indicated by Nissl staining of contiguous sections.

Figure 1- figure supplement 4

Degeneration of motor neuron fibers in phrenic nerve of GluN3B/membralin double knockout (DKO) mice.

(**A**) Primary afferent fibers, stained with anti-calcitonin gene related peptide (CGRP, red), remained intact in DKOK compared to WT mice. Axons counterstained with anti-parvalbumin (Parv, green). (**B**) Axonal degeneration of phrenic motor neurons at P5 in DKO mice, as evidenced by paucity of fibers compared to WT.

Figure 2.

Membralin transgene [Tg(membralin)] rescues GluN3B/membralin double knockout (DKO) mice.

(**A**) Generation of the transgenic construct expressing membralin. The murine prion promoter was cloned with full-length mouse membralin cDNA followed by the IRES and the EGFP sequence. The entire transgenic sequence was isolated by enzymatic digestion and used to generate Tg(membralin) mice. (**B**) DKO/Tg(membralin) mice were viable and fertile. *Left*: Genotyping by PCR showed that 3 littermates (#3, 4 and 5) from a breeding of DKO and Tg(membralin) mice were positive to DKO primers and negative to WT primers (same primers used as in Fig. 1). Of the three DKO mice, the two receiving the membralin transgene (#3 and 5, as positively identified by GFP primers) were rescued. *Right*: Weight of the 7 littermates was monitored after birth. Only DKO mouse #4, which was negative for the membralin transgene, showed weight loss after P3 and died at P5.5. Data shown here are from one representative litter (5 independent litters were analyzed with similar results). (**C**) Gene expression analysis by RT-PCR for mice #1, 3, 4 of the same litter as in **B**. Membralin transgene expression is seen in the brains of littermates #1 and 3, but not 4, whereas GluN3B is only expressed in #1. Membralin and GluN3B are not expressed in muscle samples. GAPDH is expressed in both brain and muscles of all mice and served as a positive control. (**D**) Rescued DKO/Tg(membralin) mice lived to adulthood without any sign of paresis.

Figure 2- figure supplement 1

Expression of GFP-membralin transgene in spinal cord of membralin transgenic mice.

GFP immunostaining shows expression of membralin-GFP transgene in all spinal cord layers of membralin (MEM) KO and transgenic (Tg) mice (left), but not WT mice (right).

GFP immunostaining was located predominantly in neurons, including motor neurons (arrows). Images at low (top) and high (bottom) magnification are shown from the lumbar spinal cord at P5.

Figure 2- figure supplement 2

GluN3B transgene cannot rescue GluN3B/membralin double knockout (DKO) mice.

(**A**) DNA construct used for generating GluN3B transgenic [Tg(GluN3B)] mice containing the 7 kb murine GluN3B promoter followed by murine full-length coding region for GluN3B, IRES, and GFP. (**b**) Stronger immunocytochemical signal for GluN3B signal in motor neurons of lumbar spinal cord of Tg(GluN3B) mice compared to WT mice. (**C**) Tg(GluN3B) cannot rescue DKO mice. *Left:* PCR genotyping shows one mouse (#3) among five from a DKO x Tg(GluN3B) litter was positive for DKO and GFP primers, but negative for WT primers (same primers as used in Figure 1). *Right:* Weight of the 5 littermates was monitored after birth, and DKO mouse #3, which contained the GluN3B transgene, lost weight and died at P6.

Figure 3.

Membralin KO mice die of motor neuron degeneration and consequent paresis.

(**A**) Gene trapping was used to generate membralin KO mice by inserting a trapping vector that contained a splicing acceptor sequence between exon 1 and 2 to disrupt normal RNA splicing. Primers (P1, P2, P3, red arrows) were designed to detect normal and trapped membralin transcripts. RT-PCR experiments showed that PCR products

using the P1 and P3 primer pair were only detected in WT mouse brain (lane 1), liver (lane 2), and kidney (lane 3), whereas PCR products using the P1 and P2 primers were only detected in these tissues of KO mice. (**B**) Membralin KO mice phenocopied GluN3B /membralin DKO mice and died of paresis around P5. (**C**) Lumbar motor neurons, identified by anti-Hb9 staining (*top panels*), were significantly reduced (*lower panel*) in membralin KO mice compared to WT mice (n = 3 for each group of mice, *P < 0.05, Student's *t-t*est). Data are mean + s.e.m.

Figure 4.

Cellular expression and localization of Membralin.

(**A**) Semi-quantitative RT-PCR analysis showed the expression of membralin mRNA in brain (1), spinal cord (2), lung (4), liver (5), and kidney (6), but not in heart (3), spleen (7), and muscle (8) tissues of WT mice**.** (**B**) Western blot analysis showed the expression of membralin protein in the ER fraction (ER), but not in the mitochondrial fraction (Mit) or the cytosolic fraction (Cyt), of the WT mouse brains. (**C**) Subcellular localization of Myc-tagged membralin in HEK 293 cells. Cells were transiently transfected with Myc-tagged membralin. At 48 h after transfection, localization of membralin was detected by confocal microscopy (Zeiss 710). Organelles were labeled with specific markers (anti-PDI for ER, anti-mitochondria for mitochondria, and anti-GMP130 for Golgi). Region of interest shown at higher magnification in insets (bottom right corner). Merged pictures show membralin co-localized with the ER marker, PDI.

Figure 4- figure supplement 1

Structural prediction of membralin

(**A**) Membralin's predicted structure has four transmembrane regions with termini on the same side of membrane. (**B**) The predicted glycosylation sites are also indicated by brown tree signs, which suggest the topology of the membralin on ER membrane (lumen and cytosolic side is indicated as "in" and "out", respectively).

Figure 5.

Membralin interacts with Erlin2 and regulates protein degradation.

(**A**) HEK 293T cells were transfected with control (mCherry and EGFP) or target (membralin-mCherry and Erlin2-EGFP) molecules. Individual or merged fluorescence images were shown in pre- and post-bleaching conditions. (**B**) FRET efficiency was quantified for control and target groups. All data shown are mean ± s.e.m. n=10; ***P < 0.001 by Student's *t*-test. **(C**) The interaction of membralin with Erlin2 was confirmed by co-immunoprecipitation experiments using HA-tagged Erlin2 and Myc-tagged membralin fusion proteins co-transfected into HEK 293T cells. Whole-cell lysates were immunoprecipitated with anti-Myc or IgG (negative control), and immunoblotted using anti-Erlin2. **(D**) MEFs from both WT and membralin KO mouse were transfected with HA tagged CD3-d and subjected to pulse-chase analysis of CD3-d degradation after exposing with cycloheximide (Chx). Proteins collected at the indicated time points were subjected to immunoblotting with antibodies to HA. Image shown represents example of immunoblotting, and graphs the quantification of three experiments. (n=3, *P < 0.05 by Student's *t*-test). All data shown are mean ± s.e.m.

Figure 5 - figure supplement 1

Deletion of membralin did not prolong the half life of ERAD substrate NHK.

MEFs from both WT and membralin KO mouse were transfected with HA tagged NHK and subjected to pulse-chase analysis of degradation after exposed to cycloheximide (Chx). Proteins collected at the indicated time points were subjected to immunoblotting with antibodies to HA. Image shown represent example of immunoblotting, and graphs the quantification of three experiments. All data shown are mean ± s.d.

Figure 6.

Elevated ER stress in membralin KO mice.

(A) Up-regulation of GRP78 in spinal cord of membralin KO mice. *Left*: Immunoblot analysis shows higher levels of GRP78 and ATF4 in the spinal cord of P3 membralin KO mice compared to that of littermate WT mice. Right: Increased expression level of GRP78 and ATF4 normalized to actin in membralin KO mice over WT mice. **(B)** Survival of MEFs after 24-h exposure to tunicamycin or thapsigargin determined by a cytotoxicity assay. **(C)** The expression level of GRP78, CHOP, and ATF4 in MEFs from KO and WT mice is shown after exposure to tunicamycin at different time points. Levels of CHOP and ATF4 are elevated earlier and higher in MEFs from KO than that from WT mice. A representative immunoblot is shown; graphs include data from three experiments. For each panel, data are mean ± s.e.m.; $n = 3$ for each bar; $^*P < 0.05$ by Student's *t*-test.

Figure 6 - figure supplement 1

Membralin deletion does not alter Xbp-1 splicing.

(**A**) RT-PCR assay of Xbp-1 mRNA from brain and spinal cord from membralin WT and KO mouse. (**B**) RT-PCR assay of spliced and unspliced Xbp1 mRNA from membralin WT and KO MEF cells exposed to the ER stress inducer, tunicamycin (300 nM), for the indicated times.

Supplementary File 1 Primer list for genotyping and sequencing.

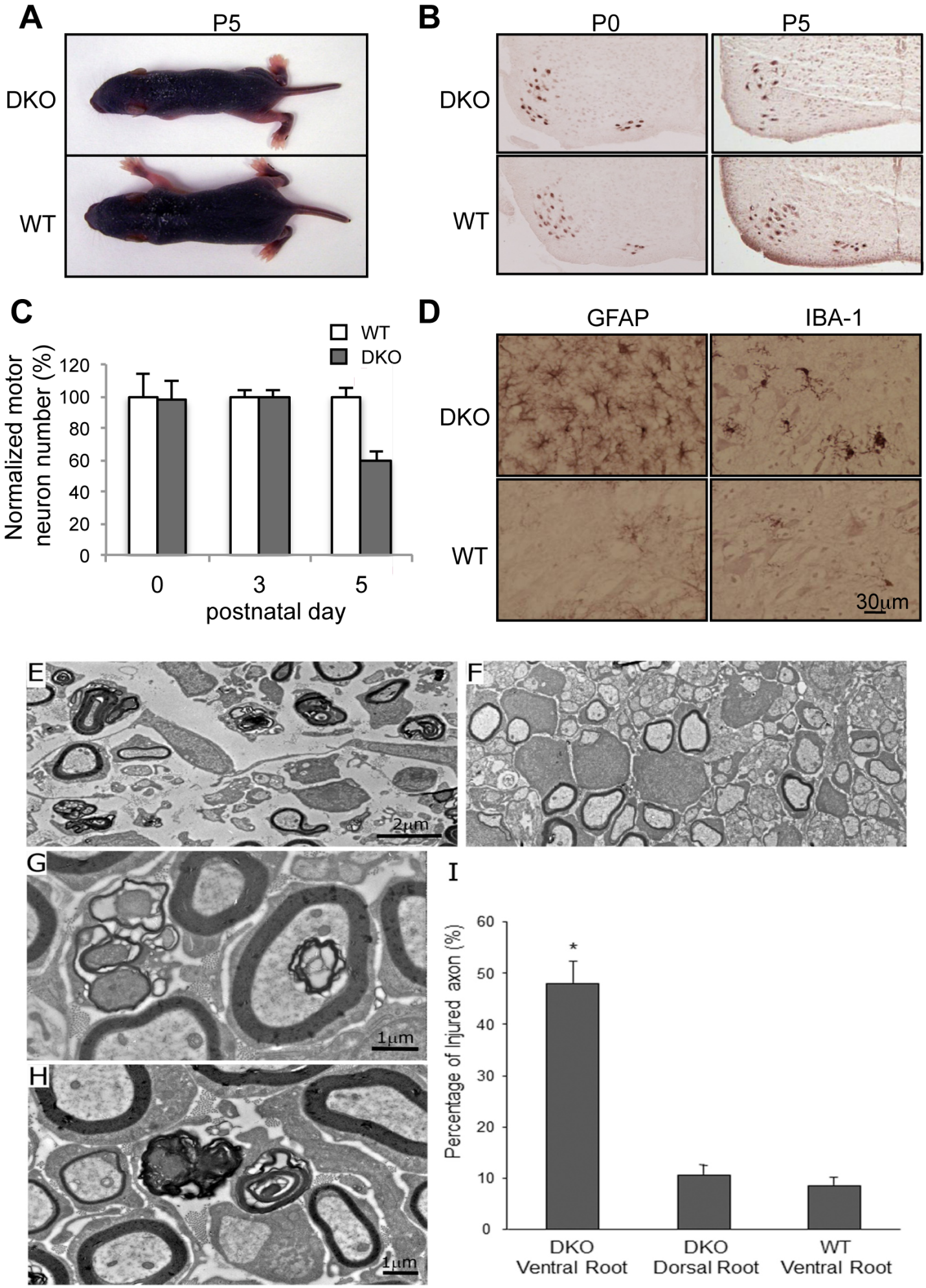
A
P5
DKO
WT
B
P0
P5
DKO
WT
C
WT
DKO
Normalized motor neuron number (%)
120
100
80
60
40
20
0
0
3
5
postnatal day
D
GFAP
IBA-1
DKO
WT
30μm
E
2μm
F
G
1μm
H
1μm
I
Percentage of Injured axon (%)
60
50
40
30
20
10
0
*
DKO Ventral Root
DKO Dorsal Root
WT Ventral Root

Figure 1

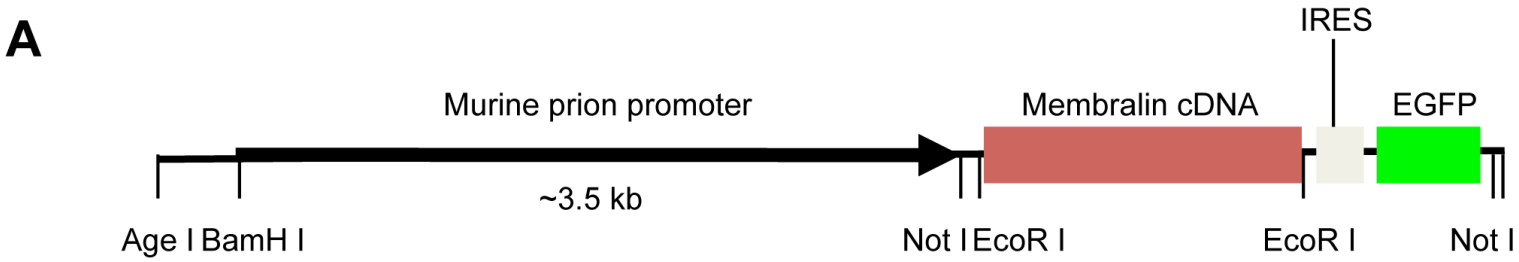
A
IRES
Murine prion promoter
Membralin cDNA
EGFP
~3.5 kb
Age I BamH I
Not I EcoR I
EcoR I
Not I

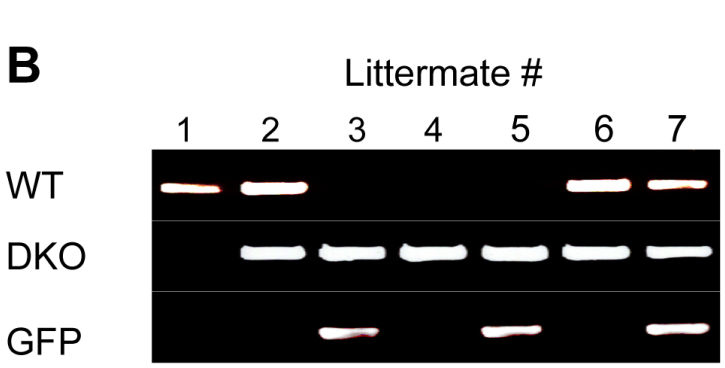
B
Littermate #
1 2 3 4 5 6 7
WT
DKO
GFP

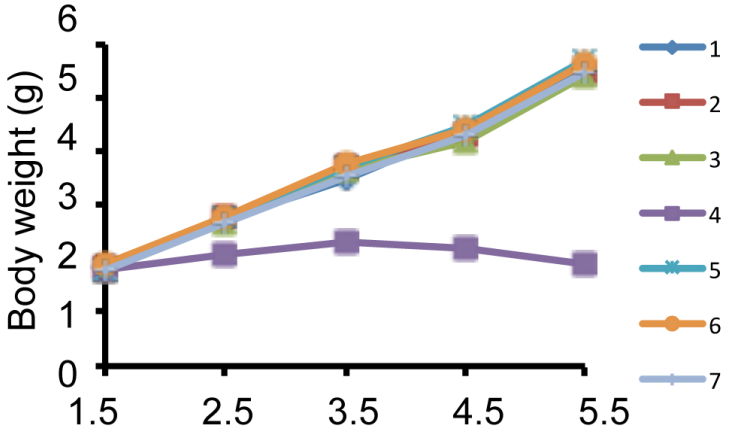
Body weight (g)
0 1 2 3 4 5 6
1.5 2.5 3.5 4.5 5.5
1 2 3 4 5 6 7

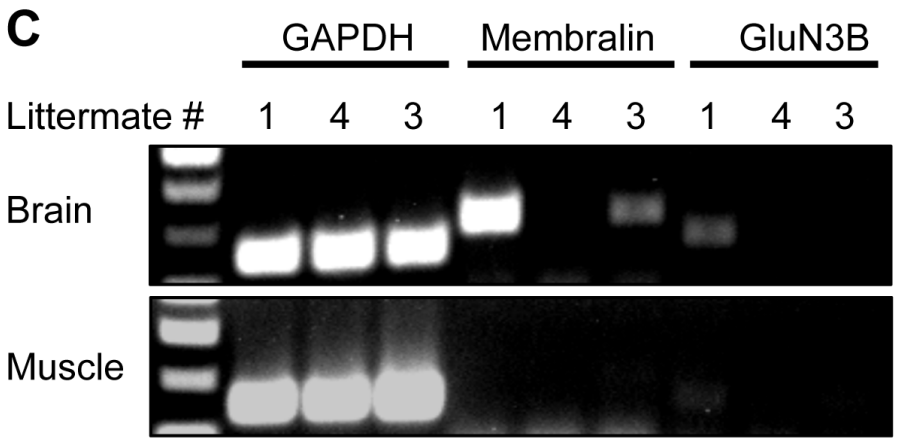
C
GAPDH
Membralin
GluN3B
Littermate # 1 4 3 1 4 3 1 4 3
Brain
Muscle

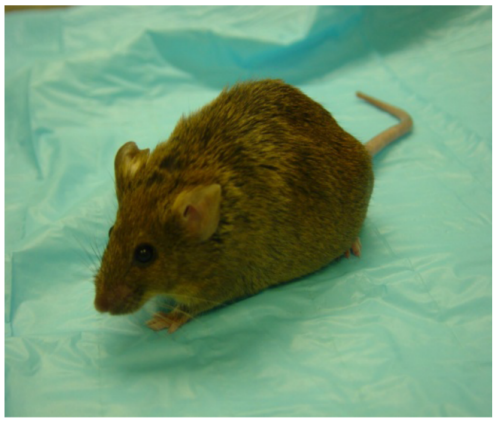
D

Figure 2

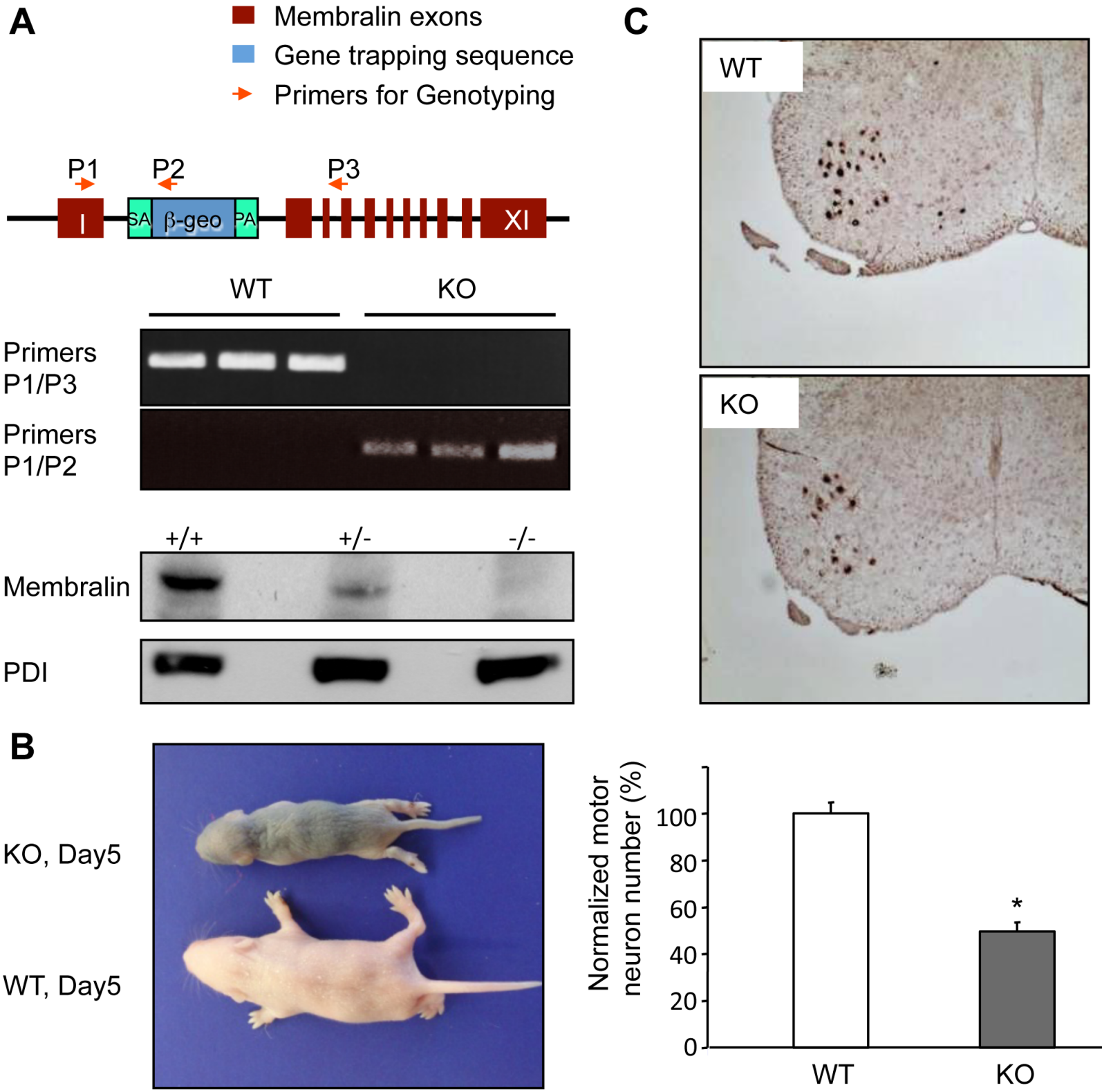
A
Membralin exons
Gene trapping sequence
Primers for Genotyping
P1
P2
P3
I
SA
β-geo
PA
XI
WT
KO
Primers P1/P3
Primers P1/P2
+/+
+/-
-/-
Membralin
PDI
C
WT
KO
B
KO, Day5
WT, Day5
Normalized motor neuron number (%)
100
80
60
40
20
0
*
WT
KO

Figure 3

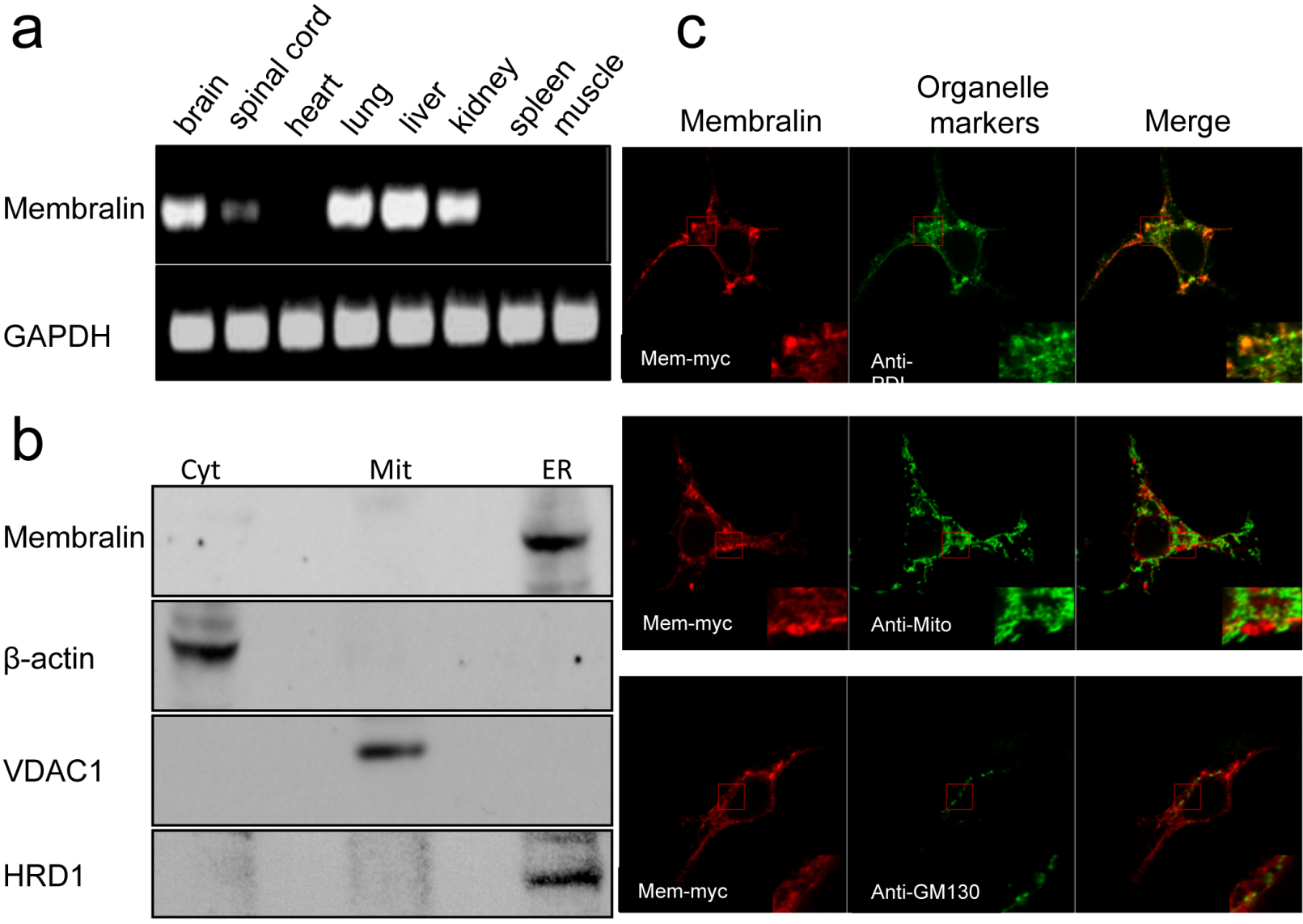
a
brain
spinal cord
heart
lung
liver
kidney
spleen
muscle
Membralin
GAPDH
b
Cyt
Mit
ER
Membralin
β-actin
VDAC1
HRD1
c
Membralin
Organelle markers
Merge
Mem-myc
Anti-
Mem-myc
Anti-Mito
Mem-myc
Anti-GM130

Figure 4

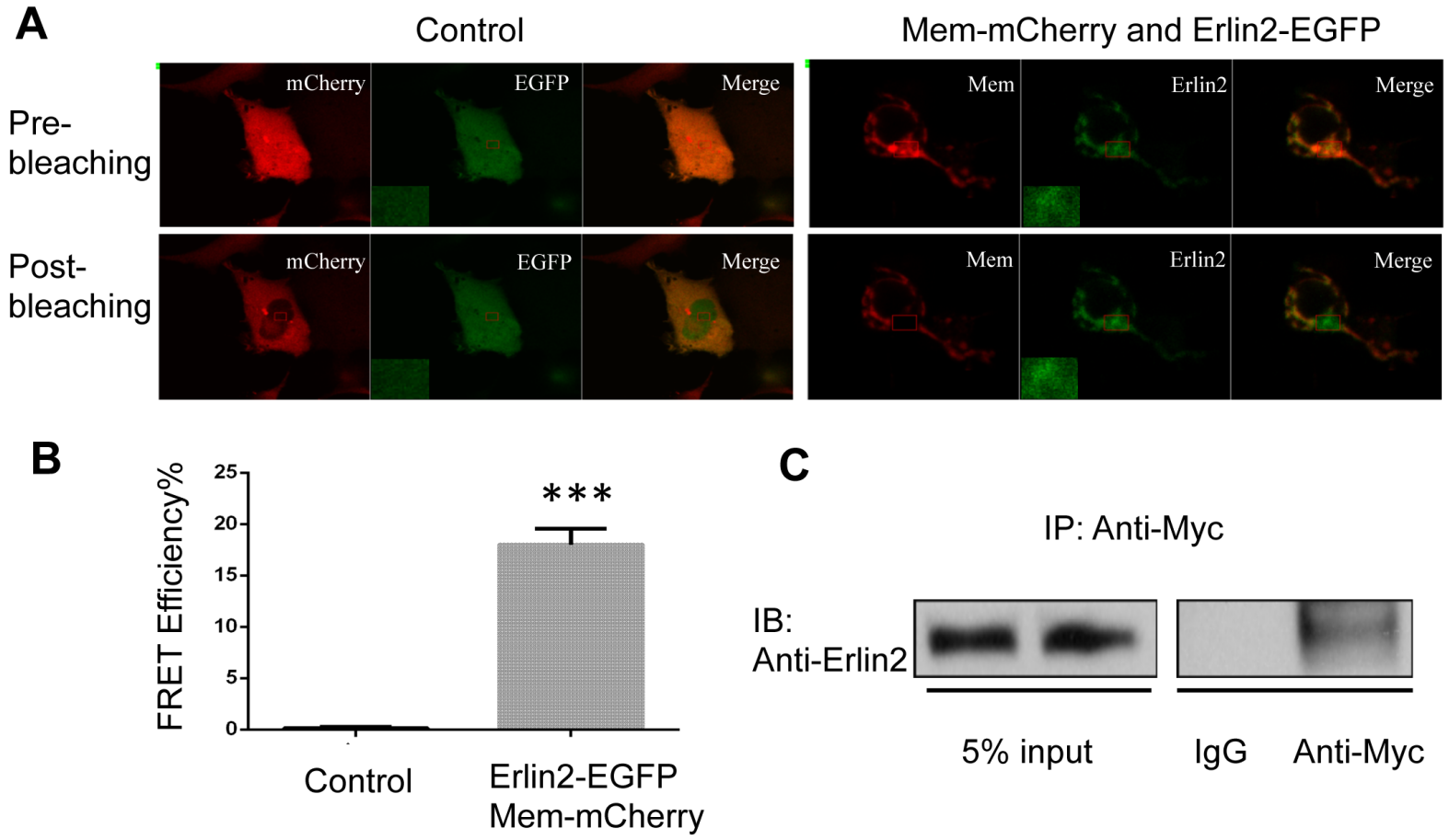
A
Control
Mem-mCherry and Erlin2-EGFP
Pre-bleaching
Post-bleaching
mCherry
EGFP
Merge
Mem
Erlin2
Merge
B
FRET Efficiency%
25
20
15
10
5
0
***
Control
Erlin2-EGFP
Mem-mCherry
C
IP: Anti-Myc
IB:
Anti-Erlin2
5% input
IgG
Anti-Myc
D
WT
KO
Chx (hr)
0 1.5 3 6 0 1.5 3 6
CD3-δ
β-actin
Relative amount CD3-δ (%)
120
100
80
60
40
20
0
WT
KO
*
*
0
3
6
Post Chx exposure (hr)

Figure 5

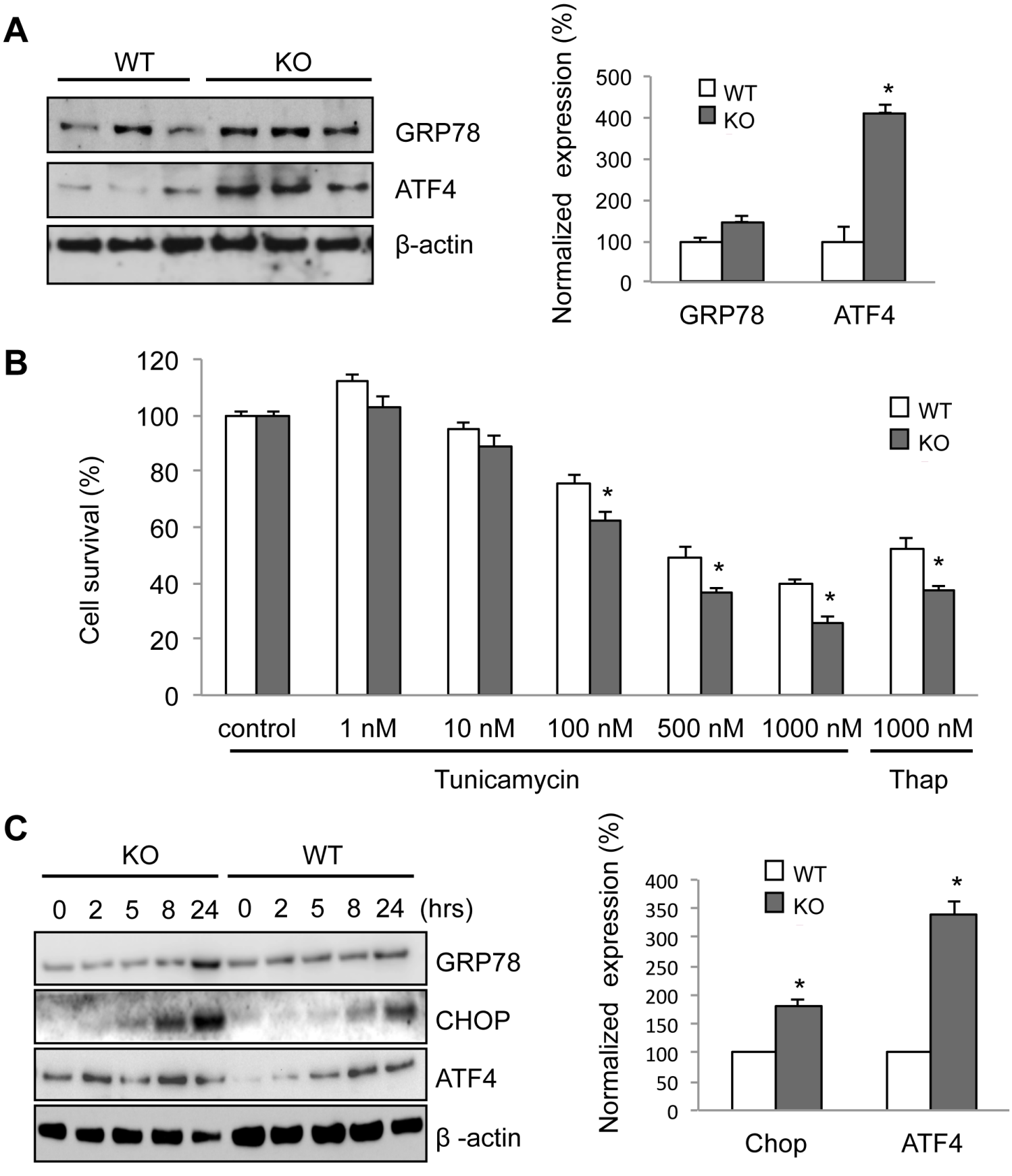
A
WT
KO
GRP78
ATF4
β-actin
Normalized expression (%)
500
400
300
200
100
0
WT
KO
*
GRP78
ATF4
B
Cell survival (%)
120
100
80
60
40
20
0
WT
KO
*
control
1 nM
10 nM
100 nM
500 nM
1000 nM
1000 nM
Tunicamycin
Thap
C
KO
WT
0 2 5 8 24 0 2 5 8 24 (hrs)
GRP78
CHOP
ATF4
β -actin
Normalized expression (%)
400
350
300
250
200
150
100
50
0
WT
KO
*
Chop
ATF4

Figure 6